



# A tabulated real-fluid model and surface density approach for LES of liquid jets primary atomization

Hesham Gaballa, Chaouki Habchi, Jean-Charles de Hemptinne

## ► To cite this version:

Hesham Gaballa, Chaouki Habchi, Jean-Charles de Hemptinne. A tabulated real-fluid model and surface density approach for LES of liquid jets primary atomization. ILASS-Americas, 32nd Annual Conference on Liquid Atomization and Spray Systems, May 2022, Madison, United States. hal-03794717

HAL Id: hal-03794717

<https://ifp.hal.science/hal-03794717>

Submitted on 3 Oct 2022

**HAL** is a multi-disciplinary open access archive for the deposit and dissemination of scientific research documents, whether they are published or not. The documents may come from teaching and research institutions in France or abroad, or from public or private research centers.

L'archive ouverte pluridisciplinaire **HAL**, est destinée au dépôt et à la diffusion de documents scientifiques de niveau recherche, publiés ou non, émanant des établissements d'enseignement et de recherche français ou étrangers, des laboratoires publics ou privés.

## **A tabulated real-fluid model and surface density approach for LES of liquid jets primary atomization**

H. Gaballa\*, C. Habchi\*, and J.C. De Hemptinne  
IFP Energies nouvelles, Institut Carnot IFPEN Transports Energie,  
1 et 4 avenue de Bois-Préau, 92852 Rueil-Malmaison, France

### **Abstract**

Modeling of fuel atomization in internal combustion engines remains a challenge for modelers. The widely used Lagrangian Discrete Droplet Method (DDM) has shown shortcomings, especially in the near nozzle region, where the primary break-up initiates from the intact liquid core. Meanwhile, Interface Capturing Methods (such as VOF, Level-Set) can be employed to investigate atomization. However, their application is limited to academic cases due to the high computational cost. Recent research has shown a remarkable performance of the Eulerian Diffuse Interface Models (DIM) based on the surface density concept for modeling liquid jet atomization in RANS and LES numerical frameworks. Accordingly, the current work proposes a more generalized approach in which a fully compressible multi-component two-phase real-fluid model (RFM) is closed by a thermodynamic equilibrium tabulation method based on a real-fluid equation of state. The RFM model is coupled to a postulated surface density equation within the LES framework for fuel atomization modeling. The Engine Combustion Network (ECN) Spray A injector cold condition is used as a reference for the proposed model validation. Simulations are carried out using the CONVERGE CFD solver. Model assessment is performed using the available ECN experimental database of fuel dispersion and interfacial surface area measurements. The LES results show that the model can capture well the fuel mass distribution in the near nozzle field, but also the interfacial surface area. In addition, the predicted drop size from simulations falls within the experimental data range. Overall, the RFM model supplemented with the surface density equation can accurately predict the fuel dispersion and primary break-up using LES under the considered subcritical condition.

---

\*Corresponding Author: chawki.habchi@ifpen.fr, hesham.gaballa@ifpen.fr

## Introduction

Fuel atomization is an essential step towards the combustion process in internal combustion engines. Indeed, the quality of the atomized spray has a significant effect on the combustion efficiency and the resultant emissions. Several atomization modeling approaches can be found in the literature with varying complexity of describing the atomization process. The widely used spray model for engineering calculations is based on the Discrete Droplet Model (DDM) approach [1], where the liquid phase is described by Lagrangian particles/blobs, whereas the gas-phase is modeled in an Eulerian framework. This approach presents various shortcomings, especially in the near nozzle region [2], where the primary break-up initiates from the intact liquid core [3]. Therefore, Eulerian modeling of the atomization process, where both liquid and gas phases are treated in an Eulerian framework, has been the subject of interest for various researchers. For instance, Interface Capturing Methods (ICM) such as the Volume of Fluid (VOF) [4] and Level-Set (LS) [5] methods have been employed for the Direct Numerical Simulation (DNS) of the atomization process [6, 7, 8]. However, due to the high computational cost of these methods, their application to industrial cases is limited. Indeed, nowadays, the fuel is injected at high Reynolds and Weber numbers, where the atomization outcome comprises extremely fine liquid structures that cannot be tracked and resolved completely by the mesh resolution. Accordingly, another alternative is the Eulerian Diffuse Interface Models (DIM) based on the surface density concept initially introduced by [9, 10] in the so called  $(\Sigma - Y)$  model. The surface density quantity ( $\Sigma$ ) represents the liquid-gas interface area per unit volume, which provide a general description of the liquid structures such as droplets or ligaments. While ( $Y$ ) stands for the liquid fraction. The  $(\Sigma - Y)$  model thus comprises two main transport equations: the liquid mass/volume fraction transport equation to track the liquid-phase dispersion and the surface density equation to model the unresolved liquid-gas interface. Then, by assuming a monodispersed spray of spherical droplets, an equivalent Sauter Mean Diameter (SMD) can be defined as ( $SMD = 6\alpha_l/\Sigma$ ), where ( $\alpha_l$ ) is the liquid volume fraction. Furthermore, the  $(\Sigma - Y)$  model is intended to provide a complete description of the atomization process from the dense near nozzle region to the diluted spray zone by switching to a Lagrangian description of the spray when it becomes sufficiently diluted, where this approach is usually termed the Eulerian-Lagrangian Spray Atomization

(ELSA) model [11, 12]. The  $(\Sigma - Y)$  model has been widely employed for modeling the fuel dispersion and atomization in diesel-like operation conditions within the Reynolds Averaged Navier-Stokes (RANS) framework [13, 14, 15]. In addition, Chesnel et al. [16] formulated the  $(\Sigma - Y)$  model within the LES framework, where the surface density equation has been postulated to describe the subgrid spray characteristics. A higher accuracy of an LES implementation of the  $(\Sigma - Y)$  model compared to its RANS counterpart has been demonstrated in previous studies [17, 18] of diesel injection. More recently, Anez et al. [19] proposed an atomization model, which couples the ICM-DNS (resolved interface) and the ELSA (unresolved interface) approaches. In this model, switching between the ICM and the ELSA approaches is implemented based on interface resolution criteria to determine whether or not the interface is well captured. Moreover, a comparison between the LES and RANS formalisms of the proposed model has revealed the superiority of the LES to recover the liquid fuel dispersion under diesel-like conditions. Thus, it can be concluded that simulation of fuel injection within the LES framework could be the best choice, especially for practical high Reynolds number conditions, where a higher accuracy of two-phase turbulence modeling is required to accurately predict the fuel dispersion and atomization processes.

Accordingly, in the current work, the Eulerian diffuse interface Real-Fluid Model (RFM) [20, 21] is supplemented with a surface density transport equation as proposed by [16] to model liquid jet atomization within the LES framework. The RFM model is a fully compressible multi-component two-phase model closed by a thermodynamic equilibrium tabulation method. The thermodynamic table is generated for binary or ternary mixtures using the in-house IFPEN Carnot library based on a vapor-liquid equilibrium (VLE) calculation coupled with a real-fluid equation of state (EoS). Such real-fluid thermodynamic modeling is indeed necessary to accurately model the fuel injection under the transcritical conditions [22, 23] encountered in modern diesel engines.

The proposed RFM model differs from previous  $(\Sigma - Y)$  models in the literature in several key points. For instance, the VLE based tabulated thermodynamic closure takes into account the subcritical phase change and the possible transition to a supercritical single-phase mixing regime. Besides, previous models assumed constant fluid properties or relied on simple EoS to model the liquid and gas phases. However, the current model is based on real-fluid EoS to capture the non-linear behavior of the

fluid properties under high-pressure conditions relevant to diesel injection.

Accordingly, the main objective of the current work is to validate the RFM model coupled with the surface density equation for atomization modeling within the LES framework. To this goal, the cold condition for the Engine Combustion Network (ECN) Spray A injector [24] is used as a reference for the proposed model validation. Model assessment is performed using the valuable ECN database of different experimental diagnostics, namely fuel dispersion and interfacial surface area measurements by means of X-ray radiography [25] and ultra small angle X-ray scattering (USAXS) technique [26], respectively. Besides, SMD experimental data [26] are also used for model validation. LES simulations are carried out using the CONVERGE CFD solver [27]. The comparison of the LES and experimental results shows that the RFM model can capture well the fuel mass distribution in the near nozzle field, but also the interfacial surface area. Besides, the predicted SMD from the simulations falls within the experimental data range. The current paper is organized as follows: Section 2 describes the RFM model, including the transport equations and the thermodynamic tabulation approach. Section 3 presents the test case setup and then the RFM model validation against the ECN experimental database. Finally, Section 4 summarizes the main conclusions along with the future perspectives.

## Real-fluid model (RFM) description

### Governing equations

The diffused interface two-phase flow model adopted in the current study is a four equation model that is fully compressible and considers multi-component in both phases under the assumptions of thermal and mechanical equilibrium. Within the LES framework, the filtered set of governing equations (1-4) expresses the conservation of mixture mass, mixture momentum, mixture internal energy, and species mass fraction, respectively.

$$\frac{\partial \bar{\rho}}{\partial t} + \frac{\partial \bar{\rho} \tilde{u}_i}{\partial x_i} = 0 \quad (1)$$

$$\frac{\partial \bar{\rho} \tilde{u}_i}{\partial t} + \frac{\partial \bar{\rho} \tilde{u}_i \tilde{u}_j}{\partial x_j} = - \frac{\partial \bar{P}}{\partial x_i} + \frac{\partial}{\partial x_j} (\bar{\tau}_{ij} + \bar{\tau}_{ij}^{sgs}) \quad (2)$$

$$\begin{aligned} \frac{\partial \bar{\rho} \tilde{e}}{\partial t} + \frac{\partial \bar{\rho} \tilde{u}_j \tilde{e}}{\partial x_j} &= - \bar{P} \frac{\partial \tilde{u}_j}{\partial x_j} + (\bar{\tau}_{ij} + \bar{\tau}_{ij}^{sgs}) \frac{\partial \tilde{u}_i}{\partial x_j} + \\ &\quad \frac{\partial}{\partial x_j} (\bar{Q}_j + \bar{Q}_j^{sgs}) \end{aligned} \quad (3)$$

$$\frac{\partial \bar{\rho} \tilde{Y}_k}{\partial t} + \frac{\partial \bar{\rho} \tilde{u}_j \tilde{Y}_k}{\partial x_j} = \frac{\partial}{\partial x_j} (\bar{J}_{k,j} + \bar{J}_{k,j}^{sgs}) \quad (4)$$

where  $(\rho, u_i, P, e)$  are the mixture's density, velocity, pressure, and specific internal energy, respectively. The viscous stress tensor  $(\tau_{ij})$  is expressed as  $(\tau_{ij} = \mu(\partial u_i / \partial x_j + \partial u_j / \partial x_i) - \frac{2}{3}\mu(\partial u_k / \partial x_k)\delta_{ij})$ , where  $(\mu)$  is the dynamic viscosity and  $\delta_{ij}$  is the Kronecker delta. The heat flux  $(Q_j)$  is defined as  $(Q_j = \lambda \frac{\partial T}{\partial x_j} + \rho \sum_k D_k h_k \frac{\partial Y_k}{\partial x_j})$ , where  $(T)$  is the mixture's temperature,  $(\lambda)$  is the thermal conductivity, and  $(D_k, h_k, Y_k)$  are the mass diffusion coefficient, specific enthalpy, and mass fraction of species k, respectively. The  $(\lambda)$  and  $(\mu)$  are computed by Chung et al. [28] correlations. The species diffusion flux  $(J_{k,j})$  is defined as  $(J_{k,j} = \rho D_k \frac{\partial Y_k}{\partial x_j})$ . The LES subgrid-scale terms denoted by the superscript (sgs) in the governing equations are modeled. The subgrid stress tensor  $(\bar{\tau}_{ij}^{sgs})$  is computed similarly to  $(\tau_{ij})$ , with the eddy viscosity assumption, replacing the molecular viscosity with the subgrid-scale viscosity  $(\mu_{sgs})$  computed by the Sigma model [29]. The subgrid species  $(J_{k,j}^{sgs})$  and heat  $(Q_j^{sgs})$  fluxes are modeled using the gradient assumption, where the molecular transport coefficients in  $(J_{k,j})$  and  $(Q_j)$  are replaced with the turbulent ones. The turbulent transport coefficients are modeled by introducing turbulent Schmidt number ( $Sc_t = 0.7$ ) and turbulent Prandtl number ( $Pr_t = 0.9$ ). The turbulent mass diffusion coefficient is computed as  $(D_t = \mu_{sgs}/\rho Sc_t)$  and the turbulent conductivity is computed as  $(\lambda_t = C_p \mu_{sgs}/Pr_t)$ , where  $(C_p)$  is the isobaric heat capacity.

The atomization is modeled by solving a transport equation for the evolution of the interfacial surface area density  $(\Sigma)$ , which is defined as the liquid-gas interface area per unit volume. The adopted equation within the LES framework is based on the proposal by [16], where the total interfacial surface area density is given by:

$$\Sigma = \Sigma_{min} + \Sigma' \quad (5)$$

The  $(\Sigma_{min})$  represents the minimum surface density that can be found for a given value of the resolved liquid volume fraction, whereas  $(\Sigma')$  stands for the subgrid level surface density. The  $(\Sigma_{min})$  is computed following [16] as:

$$\Sigma_{min} = \frac{2.4}{\Delta_{LES}} \sqrt{\bar{\alpha}_l(1 - \bar{\alpha}_l)} \quad (6)$$

where  $(\bar{\alpha}_l)$  is the resolved liquid volume fraction and  $(\Delta_{LES})$  is the filter length scale, which is estimated from the cell volume  $(V_c)$  as  $(\Delta_{LES} = V_c^{-1/3})$ . To close Eq. 5, the subgrid surface density  $(\Sigma')$  is transported as follows:

$$\frac{\partial \Sigma'}{\partial t} + \frac{\partial \tilde{u}_i \Sigma'}{\partial x_i} = \frac{\partial}{\partial x_j} \left( D_\Sigma \frac{\partial \Sigma'}{\partial x_j} \right) + \frac{\Sigma}{\tau_\Sigma} \left( 1 - \frac{\Sigma}{\Sigma_{eq}} \right) \quad (7)$$

On the RHS of Eq. 7, the first term represents the turbulent diffusion flux modeled using a gradient law closure, where the diffusion coefficient ( $D_\Sigma$ ) is computed as ( $D_\Sigma = \mu_{sgs}/\rho S c_t$ ). The second term on the RHS of Eq. 7 represents the surface production/destruction, due to turbulent flow stretching and coalescence effects, which is modeled in a restoration to equilibrium form [10, 30], where ( $\Sigma_{eq}$ ) is an equilibrium surface area density that should be reached within a characteristic time scale ( $\tau_\Sigma$ ). The ( $\tau_\Sigma$ ) is related to the turbulent time scale ( $\tau_t$ ) as ( $1/\tau_\Sigma = C_\Sigma/\tau_t$ ).

The ( $\Sigma_{eq}$ ) is evaluated as ( $\Sigma_{eq} = \Sigma_{min} + \Sigma'_{eq}$ ), where ( $\Sigma'_{eq}$ ) is computed as function of a critical Weber number ( $We_c$ ) [31] as:

$$\Sigma'_{eq} = 4 \frac{0.5(\rho_l + \rho_g)\bar{\alpha}_l(1 - \bar{\alpha}_l)k_{sgs}}{\sigma We_c}$$

where ( $k_{sgs}$ ) is the subgrid scale turbulent kinetic energy, ( $\sigma$ ) is the surface tension coefficient computed by the Macleod-Sugden correlation [32] for the considered binary system of (*n*-dodecane/nitrogen), and ( $\rho_l, \rho_g$ ) are the densities of the liquid and gas phases, respectively. The two model constants ( $C_\Sigma, We_c$ ) are set by comparison with the USAXS experimental measurements of the projected interfacial surface area.

A length scale ( $l_{32}$ ) can be defined for the liquid structures from ( $\Sigma$ ) and ( $\alpha_l$ ) as ( $l_{32} = 6\alpha_l(1 - \alpha_l)/\Sigma$ ) following [19]. This length scale definition considers on the one hand, the case of monodispersed spray of spherical droplets ( $SMD = 6\alpha_l/\Sigma$ ) and on the other hand, the case of bubbly flow with very small liquid volume fraction ( $SMD = 6(1 - \alpha_l)/\Sigma$ ).

#### *Novelty of the RFM model*

It is worth noting that the current RFM model differs from previously proposed ( $\Sigma - Y$ ) or ELSA models in several points. In the current model, the overall liquid volume/mass fraction is not directly transported, but the liquid volume fraction ( $\alpha_l$ ) is computed as  $\alpha_l = \alpha_l(T, P, Y_k, k = 1, \dots, N_s - 1, \text{where } N_s \text{ is the total number of species})$  from the thermodynamic table, which is based on the VLE calculation. Accordingly, the phase change effect on the surface density is implicitly considered through the terms ( $\Sigma_{min}$ ) and ( $\Sigma_{eq}$ ), which are dependent on ( $\alpha_l$ ). In addition, previous models have used simple EoS to compute the liquid and gas phases thermo-

dynamic and transport properties or even assumed constant properties. On the contrary, the current model is based on real fluid EoS that can capture the non-linearity of fluid properties under high pressure conditions relevant to diesel injection.

#### *Tabulated thermodynamic closure*

The fully compressible multi-component two-phase flow system, Eqs. (1-4) is closed by a tabulated real-fluid EoS adopting a local thermodynamic equilibrium hypothesis, which ensure its mathematical hyperbolicity. To consider the phase change phenomenon, the EoS is not sufficient, but a VLE calculation is also included in the RFM model. The current work proposes a pre-tabulation approach, where before the CFD simulation, a uniform thermodynamic table is generated for binary or ternary mixtures using the IFPEN-Carnot thermodynamic library. The thermodynamic library performs the VLE calculation using a robust isothermal-isobaric (TP) flash [33] coupled to a real-fluid EoS. The tabulated properties include the thermodynamic equilibrium density, internal energy, fluid-phase state and composition, and necessary thermodynamic derivatives as heat capacity, sound speed, and transport properties. The thermodynamic table axes are the temperature ( $T$ ), pressure ( $P$ ) and species mass fraction ( $Y_k, k = 1, \dots, N_s - 1$ , where  $N_s$  is the total number of species). The RFM tabulation approach can be used to simulate binary [20, 34], and ternary [21] mixtures. During the simulation, the required tabulated quantities are interpolated as function of ( $T, P, Y_k$ ) using the Inverse Distance Weighting method (IDW) [35]. The thermodynamic table is coupled with CONVERGE CFD solver [27] as detailed in [20, 21, 34]. The thermodynamic table is used during the simulation for two main tasks as follow:

- Properties look-up: compute the thermodynamic and transport properties, the phase state and composition based on ( $T, P, Y_k, k = 1, \dots, N_s - 1$ ) obtained from the flow solver.
- Temperature reverse look-up: compute the temperature ( $T$ ) from ( $e, P, Y_k, k = 1, \dots, N_s - 1$ ) provided by the flow solver.

The tabulated thermodynamic closure is achieved using the Peng-Robinson (PR) [36] EoS for the (*n*-dodecane/nitrogen) binary system involved in the ECN spray A simulation. Volume translation [37] has been used to improve the accuracy of the liquid phase density predicted by the cubic PR EoS.

## Results and discussion

The current study is based on the cold condition ECN spray A test case, where liquid n-dodecane ( $C_{12}H_{26}$ ) is injected into gaseous nitrogen ( $N_2$ ) at the conditions listed in Table 1. The test case setup is described in the next section, followed by the RFM-LES results comparison against the ECN experimental data.

Fuel	<i>n</i> -dodecane
Injection pressure (MPa)	150
Injection temperature (K)	343
Ambient temperature (K)	303
Ambient pressure (MPa)	2
Ambient density (kg/m <sup>3</sup> )	22.8
Ambient composition	Pure $N_2$

Table 1: Injection and ambient conditions of ECN spray A cold condition

### Numerical setup

The employed numerical setup comprises a rectangular chamber, which is 20 mm in the stream-wise direction and 10 mm in the lateral directions. The nozzle outlet diameter is 0.0894 mm corresponding to spray A injector serial #210675 [38]. The grid structure is depicted in Fig. 1, where the base grid size is 400  $\mu\text{m}$  located at the outer edge of the domain, while several mesh refinement levels have been employed to achieve a minimum cell size of  $\sim 6 \mu\text{m}$ . Thus, the nozzle outlet diameter is discretized with about 15 cells.

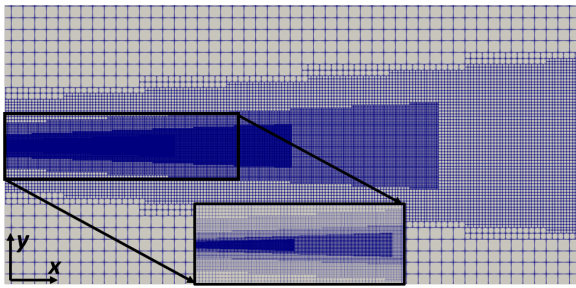


Figure 1: Computational domain with the grid structure at the central cut section. The insert shows a zoom of the refined mesh in the near-nozzle exit region.

First, a grid convergence study has been performed by further increasing the grid refinement levels in the different mesh embedding regions, resulting in three grids with a total mesh count of 3 M

(Grid 1), 16 M (Grid 2), and 21 M (Grid 3) cells, respectively. The injection conditions are applied at the domain inlet (nozzle outlet) by an inlet boundary condition (BC), based on a time-dependent mass-flow rate profile obtained from CMT [39], which allows to partially reproduce the in-nozzle flow and the needle motion effects [13, 40]. Thus, the injector internal flow was not simulated. Besides, a synthetic turbulence generator has been used to superimpose turbulent fluctuations over the inflow velocity profile following the method by [41]. According to [18], the turbulent intensity ( $I$ ) ranges between 3% to 5% for the cold spray A case, with ( $I = 3\%$ ) showing the best match of the fuel dispersion with the experiments. Thus, ( $I = 3\%$ ) has been adopted in the current study and the minimum length-scale of the imposed fluctuations was taken as twice the minimum cell size. A no-slip boundary condition is applied at the wall around the nozzle outlet (on left side of the chamber). All the rest of the domain boundaries are outlets with a pressure boundary condition of 2 MPa. LES simulations are carried out using the RFM model described above. The numerical solution of the transport equations is based on a modified Pressure Implicit with Splitting of Operator (PISO) algorithm [42] for the pressure-velocity coupling. The spatial discretization is second-order accurate using a central difference scheme. The time integration is achieved by a second-order Crank-Nicolson scheme for the momentum equation and a first-order implicit Euler scheme for the rest of the equations. The time step is around 2-3 ns and adjusted automatically based on a maximum acoustic Courant number of 0.5.

### Spray dispersion

The RFM model predictions of the spray dispersion is validated using the ECN experimental data [43], which include the Projected Mass Density (PMD) [25], Transverse Integrated Mass (TIM) [44], and Liquid Volume Fraction (LVF) [45]. The LES results are time-averaged between 0.4 and 1 ms after the start of injection (i.e. during the quasi-steady period) to be compared with the experiments. A first validation is performed using the PMD, which represents a path length-integrated measure of the fuel density along the X-ray beam path through the spray. Line of sight integration of the simulation results of the fuel density is carried out and compared with the experimental results as shown in Fig. 2. It can be seen that a qualitatively good agreement is achieved between the simulation and the experiment for the fuel dispersion in the near nozzle region (first 6 mm).

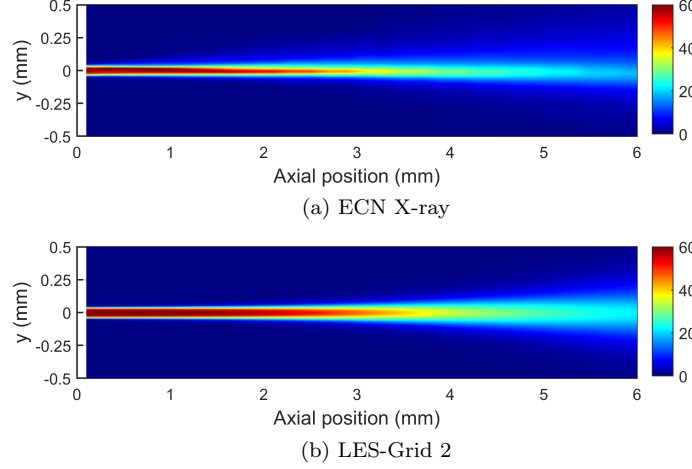


Figure 2: Projected mass density ( $\mu\text{g}/\text{mm}^2$ ) distributions.

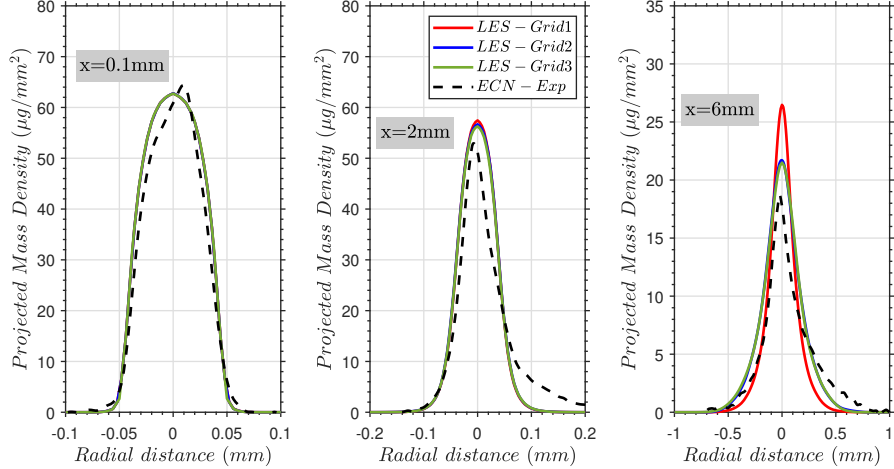


Figure 3: Projected mass density radial profiles at axial distances of 0.1 mm, 2 mm, and 6 mm from the nozzle exit.

In addition, for more quantitative validation, the projected mass density radial profiles are compared at three different axial positions ( $x = 0.1, 2, 6 \text{ mm}$ ) from the nozzle outlet as depicted in Fig. 3. Overall, the model results of the PMD radial distributions show a good agreement with the experimental data at the different axial positions, especially when the grid 2 and 3 are employed. Indeed, it can be seen the grid impact on the obtained results, especially at ( $x = 6 \text{ mm}$ ), where the predicted PMD tends to better match the experimental one as the mesh is further refined. A grid independent solution can be achieved with grid 2, which has been used for further calculations.

Another useful quantity is the TIM, which is ob-

tained from the integral of the projected mass density across the transverse position at a particular axial location. A comparison between the TIM distribution between the simulation and the experimental data is shown in Fig. 4. The simulation result fairly agrees with the experimental data in the first 5 mm. Then the predicted TIM tends to be overestimated as the axial distance increases, indicating that the fuel radial distribution is not accurately captured.

In addition to the PMD and the TIM, the LVF is used for validation. The experimental LVF is obtained by a tomographic reconstruction [45] of the X-ray radiography data. A comparison between the simulation LVF profile along the spray axis and reconstructed LVF is shown in Fig. 5. It is worth

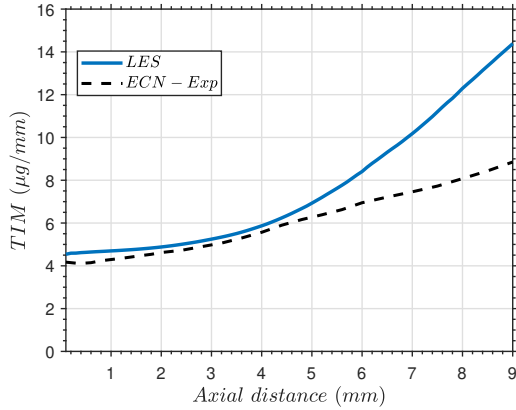


Figure 4: Numerical and experimental transverse integrated mass (TIM) along the spray axis.

noting that the experimental profile is only available in the first 12 mm. The comparison shows that the simulation result match with great accuracy the experimental profile, reproducing the intact liquid core ( $LVF > 0.9$ ) and the LVF decay along the spray center-line. It also shows that the model can capture well the fuel dispersion from the dense near-nozzle region to more diluted zones of the spray.

The performed assessment based on the PMD, TIM, and LVF data shows that the RFM model can capture well the fuel dispersion with sufficient accuracy under the considered conditions.

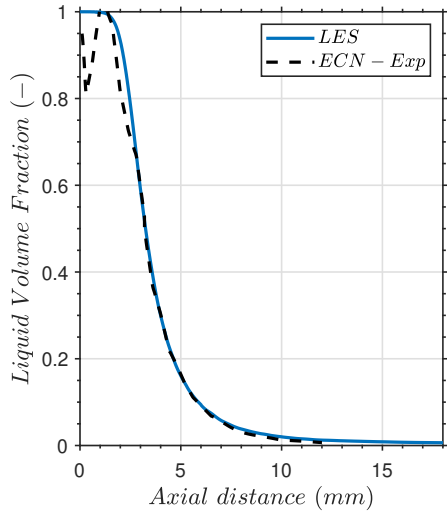


Figure 5: Computed and measured liquid volume fraction (LVF) along the spray axis.

### Spray atomization

Atomization modeling assessment is carried out in the current section using the USAXS measurements of the projected interface surface area density [15, 26] and SMD experimental data [26]. It is worth recalling the surface density equation includes two modeling constants ( $C_\Sigma, We_c$ ) that need to be calibrated against DNS or experimental data. The USAXS experimental data are used in the current work to fix the two model constants. The constant ( $C_\Sigma$ ) is set to 1, as it has been shown in previous studies [18, 15], that a value in the vicinity of one is sufficient to match the experimental data. Besides, the critical Weber number ( $We_c$ ) is set to 1.5, which is the value proposed by [46] based on two-phase DNS studies. Accordingly, the two model constants ( $C_\Sigma = 1, We_c = 1.5$ ) are used and assessed against the USAXS experimental data. The USAXS measurements represent the projected surface area density along the spray centerline. Thus, the time-averaged numerical surface area density is integrated along the spray depth to be compared with the experiments. The comparison of the numerical and experimental projected surface area density is depicted in Fig. 6.

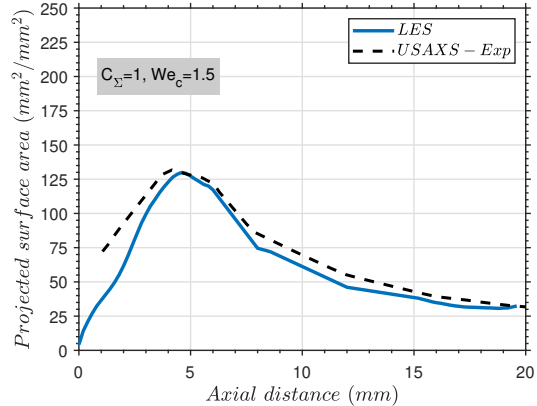


Figure 6: Computed and measured projected surface area along the spray axis.

Overall, the experimental surface area density is well reproduced by the model with the two constants ( $C_\Sigma = 1, We_c = 1.5$ ). Although, some mismatches can be observed, however the experimental surface density profile peak and decay along the spray centerline is fairly recovered by the model. Further decreasing the mismatches between the numerical and experimental projected surface density could be achieved by tuning ( $C_\Sigma, We_c$ ).

Simulation results are also compared with available SMD measurements that are obtained by combining the X-ray radiography and the USAXS measurements [26]. A quantitative comparison of SMD radial profiles at different axial positions from the time averaged LES results and the experimental data is depicted in Fig. 7.

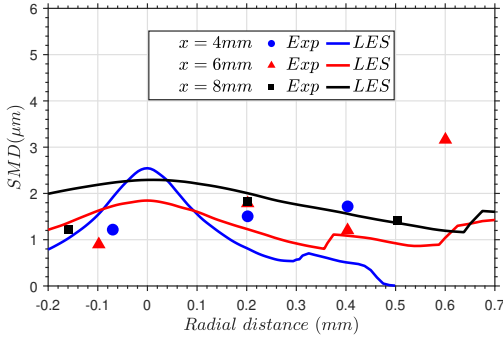


Figure 7: Computed and measured SMD radial profiles at axial distances of 4 mm, 6 mm, and 8 mm from the nozzle exit.

It can be seen the drop size from simulations fall into the same range of the experimental data. Besides, the simulation results tends to match better the experimental data at longer axial distance from the nozzle exit, where the intact liquid core vanishes and the spray is more diluted, for instance at ( $x = 8 \text{ mm}$ ). It is also worth noting that the average droplet size is quite small (less than  $3 \mu\text{m}$ ), which could justify that coupling with the Lagrangian approach was not considered in the current study.

## Conclusion

In this paper, fuel dispersion and atomization in diesel-like operating conditions have been investigated using the real-fluid model (RFM) [20, 21]. In the current study, the RFM model is supplemented with a surface density transport equation for atomization modeling within the LES framework. The cold condition of the ECN spray A injector is taken as a reference for model validation taking advantage of the available ECN experimental database. Comparing the LES simulations results with the different experimental data, including PMD, TIM, and LVF has shown a good agreement, which indicates that the RFM model can accurately capture the fuel dispersion under the considered conditions.

In addition, the atomization model assessment is carried out by comparing the model results against the experimental projected surface area density along the spray centerline and the SMD radial pro-

files. The obtained results show that the RFM model coupled with the surface density equation can reproduce the experimental projected surface density along the spray axis with sufficient accuracy. Besides, further comparison with the SMD measurements has demonstrated that the model prediction for the SMD falls within the experimental data range.

Overall, it can be concluded that the proposed RFM model coupled with the surface density model can accurately predict the fuel dispersion and primary atomization under the considered conditions.

Although it has been shown that the spray can be accurately modeled, however coupling with the internal injector flow is indeed an essential step to be done, especially for cavitating fuel injectors, where the cavitation development has a significant effect on the subsequent fuel dispersion and atomization.

## Acknowledgment

This project has received funding from the European Union Horizon 2020 Research and Innovation programme. Grant Agreement no. 861002 for the EDEM project.

## References

- [1] J. K. Dukowicz. *Journal of Computational Physics*, 35(2):229–253, 1980.
- [2] Q. Xue, M. Battistoni, C. F. Powell, D. E. Longman, S. P. Quan, E. Pomraning, P. K. Senecal, D. P. Schmidt, and S. Som. *International Journal of Multiphase Flow*, 70:77–88, 2015.
- [3] B. M. Devassy, C. Habchi, and E. Daniel. *Atomization and Sprays*, 25(1):47–80, 2015.
- [4] C. W. Hirt and B. D. Nichols. *Journal of Computational Physics*, 39(1):201–225, 1981.
- [5] M. Sussman, P. Smereka, and S. Osher. *Journal of Computational Physics*, 114(1):146–159, 1994.
- [6] T. Ménard, S. Tanguy, and A. Berlemont. *International Journal of Multiphase Flow*, 33(5):510–524, 2007.
- [7] J. Shinjo and A. Umemura. *International Journal of Multiphase Flow*, 36(7):513–532, 2010.
- [8] M. Herrmann. *Atomization and Sprays*, 21(4):283–301, 2011.
- [9] A. Vallet and R. Borghi. *Comptes Rendus de l'Académie des Sciences - Series IIB*

- Mechanics-Physics-Astronomy, 327(10):1015–1020, 1999.
- [10] Ariane Vallet, A. A. Burluka, and R. Borghi. *Atomization and Sprays*, 11(6):24, 2001.
- [11] G. Blokkel, B. Barbeau, and R. Borghi. *SAE Technical Paper Series*. Warrendale, PA, United States, 2003.
- [12] R. Lebas, G. Blokkel, P.-A. Beau, and F.-X. Demoulin. *SAE Technical Paper Series*. Warrendale, PA, United States, 2005.
- [13] J. M. Garcia-Oliver, J. M. Pastor, A. Pandal, N. Trask, E. Baldwin, and David P. Schmidt. *Atomization and Sprays*, 23(1):71–95, 2013.
- [14] J. M. Desantes, J. M. Garcia-Oliver, Jose M. Pastor, and A. Pandal. *Atomization and Sprays*, 26(7):713–737, 2016.
- [15] A. Pandal, J. M. Pastor, R.l Payri, A. Kastengren, D. Duke, K. Matusik, J. S. Giraldo, C. Powell, and D. Schmidt. *SAE International Journal of Fuels and Lubricants*, 10(2):423–431, 2017.
- [16] J. Chesnel, J. Reveillon, T. Menard, and F.-X Demoulin. *Atomization and Sprays*, 21(9):711–736, 2011.
- [17] J. M. Desantes, J. M. Garcia-Oliver, J. M. Pastor, A. Pandal, B. Naud, K. Matusik, D. Duke, A. Kastengren, C. Powell, and D. P. Schmidt. *28th Conference on Liquid Atomization and Spray Systems*, Valencia, Spain, 2017.
- [18] J. M. Desantes, J. M. Garcia-Oliver, J. M. Pastor, I. Olmeda, A. Pandal, and B. Naud. *International Journal of Multiphase Flow*, 127:103272, 2020.
- [19] J. Anez, A. Ahmed, N. Hecht, B. Duret, J. Reveillon, and F. X. Demoulin. *International Journal of Multiphase Flow*, 113:325–342, 2019.
- [20] S. Jafari, H. Gaballa, C. Habchi, and J.-C. de Hemptinne. *Energies*, 14(18):5621, 2021.
- [21] H. Gaballa, S. Jafari, C. Habchi, and J.-C. de Hemptinne. *International Journal of Heat and Mass Transfer*, 189:122671, 2022.
- [22] S. Yang, P. Yi, and C. Habchi. *International Journal of Multiphase Flow*, 122:103145, 2020.
- [23] P. Yi, S. Yang, C. Habchi, and R. Lugo. *Physics of Fluids*, 31(2):026102, 2019.
- [24] Engine Combustion Network (ECN), available at. <https://ecn.sandia.gov/>.
- [25] A. L. Kastengren, F.Z Tilocco, D. Duke, and C. F. Powel. *12th Triennial International Conference on Liquid Atomization and Spray Systems*, 2012.
- [26] A. Kastengren, J. Ilavsky, J. P. Viera, R. Payri, D. J. Duke, A. Swantek, F. Z. Tilocco, N. Sovis, and C. F. Powell. *International Journal of Multiphase Flow*, 92:131–139, 2017.
- [27] K.J. Richards, P.K. Senecal, and E. Pomraning. CONVERGE 3.0, Convergent Science, Madison, WI (2021).
- [28] T. H. Chung, M. Ajlan, L. L. Lee, and K. E. Starling. *Industrial & Engineering Chemistry Research*, 27(4):671–679, 1988.
- [29] F. Nicoud, H. B. Toda, O. Cabrit, S. Bose, and J. Lee. *Physics of Fluids*, 23(8):085106, 2011.
- [30] R. Lebas, T. Menard, P. A. Beau, A. Berlemont, and F. X. Demoulin. *International Journal of Multiphase Flow*, 35(3):247–260, 2009.
- [31] B. Duret, J. Reveillon, T. Menard, and F. X. Demoulin. *International Journal of Multiphase Flow*, 55:130–137, 2013.
- [32] B. E. Poling, J. M. Prausnitz, and J. P. O'Connell. *The properties of gases and liquids*. McGraw-Hill, New York, 2001.
- [33] M. L. Michelsen. *Fluid Phase Equilibria*, 9(1):21–40, 1982.
- [34] S. Jafari, H. Gaballa, C. Habchi, J.-C. de Hemptinne, and P. Mougin. *The Journal of Supercritical Fluids*, p. 105557, 2022.
- [35] C. Ware, W. Knight, and D. Wells. *Computers & Geosciences*, 17(7):985–993, 1991.
- [36] D.-Y. Peng and D. B. Robinson. *Industrial & Engineering Chemistry Fundamentals*, 15(1):59–64, 1976.
- [37] A. Pénéroux, E. Rauzy, and R. Fréze. *Fluid Phase Equilibria*, 8(1):7–23, 1982.
- [38] Engine Combustion Network (ECN), Spray A geometry, <https://ecn.sandia.gov/diesel-spray-combustion/target-condition/spray-a-nozzle-geometry>.
- [39] CMT, Virtual Injection Rate Generator, <https://www.cmt.upv.es/#/ecn>.

- [40] J. M. Desantes, J. M. Garcia-Oliver, J. M. Pastor, A. Pandal, E. Baldwin, and D. P. Schmidt. *International Journal of Multiphase Flow*, 80:89–99, 2016.
- [41] L. Davidson and M. Billson. *International Journal of Heat and Fluid Flow*, 27(6):1028–1042, 2006.
- [42] R.I Issa. *Journal of Computational Physics*, 62(1):40–65, 1986.
- [43] ECN-Near-nozzle mixture derived from x-ray radiography, <https://ecn.sandia.gov/rad675>.
- [44] Alan L. Kastengren, Christopher F. Powell, Yujie Wang, Kyoung-Su Im, and Jin Wang. *Atomization and Sprays*, 19(11):1031–1044, 2009.
- [45] Lyle M. Pickett, Julien Manin, Alan Kastengren, and Christopher Powell. *SAE International Journal of Engines*, 7(2):1044–1053, 2014.
- [46] F-X Demoulin, J. Reveillon, B. Duret, Z. Bouali, P. Desjonquieres, and T. Menard. *Atomization and Sprays*, 23(11):957–980, 2013.